Compound Microgrid Installation Operation Planning of a PEFC and Photovoltaics with Prediction of Electricity Production Using GA and Numerical Weather Information

Keywords: Microgrid, Photovoltaics, Operation Planning, Genetic Algorithm, Numerical Weather Information

Shin-ya OBARA* and Abeer Galal El-Sayed*

*Department of Electrical and Electronic Engineering, Power Engineering Lab., Kitami Institute of Technology, 165 Kouen-cho, Kitami, HOKKAIDO 0908507, Japan

e-mail: obara@indigo.plala.or.jp

Abstract

A fuel cell microgrid with photovoltaics effectively reduces greenhouse gas emission. A system operation optimization technique with photovoltaics and unstable power is important. In this paper, the optimal operation algorithm of this compound microgrid is developed using numerical weather information (NWI) that is freely available. A GA (genetic algorithm) was developed to minimize system fuel consumption. Furthermore, the relation between the NWI error characteristics and the operation results of the system was clarified. As a result, the optimized operation algorithm using NWI reduced the energy cost of the system.

Keywords (6 keywords): PEFC, Compound microgrid, Operation planning, Photovoltaics, Genetic algorithm, Numerical weather information

1. Introduction

An energy supply system using a microgrid constitutes the optimal system for energy demand. Therefore, its use as a clean energy supply technique is expected to spread [1-3]. A microgrid using a PEFC (proton exchange membrane fuel cell) may become the mainstream of future distributed energy. In addition, the application of green energy to a microgrid is desired. Accordingly, this paper examines the PEFC and a

photovoltaics compound system. Power can be supplied to a grid from each PEFC and photovoltaic component in this system. The hydrogen supply method to the PEFC assumes that the steam reforms the LPG (liquefied petroleum gas). However, the power generation output characteristics and PEFC exhaust heat with a steam reformer are nonlinear with a load factor [4]. Furthermore, although the power and exhaust heat of the proposed system are utilized effectively, battery installation and a heat storage tank are planned. Consequently, the operation plan of the proposed microgrid must be optimized as a nonlinear system considering electricity and heat storage. Concerning operation optimization of a nonlinear system with heat storage, we have summarized the use of a GA (genetic algorithm) [5-7]. In addition, it is necessary to predict unstable photovoltaic electricity production for every sample time while optimizing operation of a compound microgrid with a PEFC and photovoltaics. Accordingly, numerical weather information (NWI) is used to predict photovoltaic electricity production [8, 9]. Anyone can obtain NWI in Japan through the Internet. However, there is an error in the photovoltaic electricity production calculated using NWI compared to using the actual meteorological data. Consequently, the operation plan of the system using the NWI differs from operation under actual weather. The cause of this difference in operation is not addressed in this paper. Instead, the relation between the NWI error and the operation results of the system is clarified. It is shown that installing the operation optimization algorithm using NWI is important for operation of a PEFC microgrid with photovoltaics. The objective of this study is to develop an analysis algorithm to optimize operation of a PEFC microgrid with green energy.

2. System Configurations

2.1 PEFC and photovoltaics compound microgrid

Figure 1 shows a scheme of a compound microgrid with PEFC and photovoltaics. The compound microgrid consists of a power system and a heat system. Here, the power system is not connected with a commercial power system. The power from a PEFC and a solar cell can be supplied simultaneously to a microgrid. Moreover, these power sources can accumulate electricity using a battery. The hydrogen (reformed gas) supplied to a PEFC is produced from LPG (liquefied petroleum gas) using a steam reformer.

Each piece of equipment of the power system and the heat system is operated by a system controller. The photovoltaic electricity production for every sample time in a target day is predicted using the NWI (the

amount of solar radiation and outdoor air temperature) obtained by the system controller at 0:00 on the target day. Based on this prediction result, the optimal system operation on the target day is planned by the system controller. The objective given to the system controller is to minimize fuel (LPG) consumption. As Fig. 1 shows, fuel is consumed by a PEFC and a boiler in the proposed system. The optimization analysis of the operation plan in this paper considers operation of a power system and a heat system. The NWI used for analysis is the information obtained at 0:00 on a target day. Therefore, the NWI does not match actual meteorological data. If a system is employed according to the first optimization plan (the plan is made at 0:00 on the target day), then depending on the magnitude of this error, the fuel consumption may get worse. For example, the operation hours of a PEFC and a boiler may be extended under the actual weather conditions. Investigating the relation between the NWI error and system fuel consumption evaluates the operation optimization algorithm using NWI.

2.2 System operation

Figure 2 shows power demand (a) on a representative day, heat demand (d), electricity production and exhaust heat of PEFC (b), (e), the operation model of a battery (c) and the operation model of heat storage and the boiler (f). Predicted photovoltaic electricity production based on the NWI obtained at 23:00 on a representative day is shown in Figs. 2 (a) and (d). Furthermore, the photovoltaic electricity production obtained under actual weather conditions at each time is shown in this figure.

The relation between the load factor and power generation efficiency of a PEFC with a reformer, load factor and heat generation efficiency is nonlinear. Figure 3 shows the relation of the load factor and power generation efficiency of a home fuel cell with an LPG reformer released by Tokyo Gas Co. Ltd. [10]. As shown in Fig. 3 (a), power generation efficiency also falls according to load decreases. Therefore, the PEFC operates well under high load. Accordingly, as shown in Fig. 2 (b), it is desirable to operate the PEFC near its maximum efficiency point. When the PEFC is operated near the maximum efficiency point, exhaust heat of the PEFC is an output characteristic, shown in Fig. 2 (e). Operation of the PEFC in the periods from t_0 to t_1 and t_8 to t_9 in Figs. 2 (b) and (e) are the optimal operation plan based on predicted solar power shown in Figs. 2 (a) and (d). On the other hand, operation of PEFC in the periods from t_2 to t_4, t_7 to t_8 and t_{10} to t_{11} in Figs. 2 (b) and (e) covers the photovoltaic shortage compared to the actual solar power (the

actual solar power is smaller than the predicted solar power), as shown in Figs. 2 (a) and (d). When there is little actual solar power compared to the predicted solar power, additional PEFC operation is required. In this case, as shown in Figs. 2 (c) and (f), battery, heat storage tank and boiler operations change. Accordingly, the relation between the magnitude of the difference of the predicted solar power and the actual solar power, and the fuel consumption of the system is investigated. By considering this result, the influence of the NWI error on the system operation plan can be identified.

3. Analysis method

3.1 Power system

3.1.1 Photovoltaics

In this paper, installation of the polycrystalline silicon solar module of area S_S is assumed. The average production of electricity $P_{s,t}$ of the solar module from sample time t to $t+1$ on a representative day is calculated as shown in Fig. (1). R_T in Eq (1) is the temperature coefficient, and when the temperature $T_{c,t}$ of the solar cell rises, power generation efficiency will fall. T_o is a reference temperature, and η_S is the power generation efficiency under T_o. The temperature $T_{c,t}$ of the solar cell is calculated from the specific heat of the polycrystalline silicon and the amount of solar radiation at sampling time t. When the intensities of direct solar and sky solar radiation are expressed by $H_{D,t}$ and $H_{M,t}$, respectively, among the solar radiation input into the acceptance surface, $P_{s,t}$ will be calculated by Eq. (1).

Direct solar insolations and sky solar radiation are used for power generation in a flat solar cell. Global-solar-radiation intensity, direct solar radiation intensity, and horizontal sky solar radiation intensity at time t (t =0.1, 2, …, 23) are expressed with $I_{H,t}$, $I_{D,t}$ and $I_{M,t}$, respectively. $I_{H,t}$ and $I_{D,t}$ can be determined from the NWI. Moreover, $I_{M,t}$ can be calculated using $I_{H,t}$ and $I_{D,t}$. The incidence angle θ to the acceptance surface of sunlight is calculated using Eq. (2). Here, φ, δ, and ω show the latitude of a setting point, the solar celestial declination, and hour angle, respectively, while Equation (3) is a calculation formula for the sky solar radiation component $H_{D,t}$.

$$P_{s,t} = S_S \cdot \eta_S \cdot \left(H_{D,t} + H_{M,t}\right) \cdot \left\{1 - \left(T_{c,t} - T_o\right) \cdot \left(R_T / 100\right)\right\} \quad (1)$$

$$\sin\theta = \cos\varphi \cdot \sin\delta - \sin\varphi \cdot \cos\omega \cdot \cos\delta \quad (2)$$

$$H_{D,t} = I_{D,t} \cdot \cos\theta \quad (3)$$

Equation (4) calculates the incidence sky solar radiation component $H_{M,t}$ of the solar cell. The first term on the right-hand side of Eq. (4) is the air solar radiation component; the second term is the reflective solar radiation component; β is the angle of gradient of the acceptance surface by Eq. (5); and ρ is the reflection factor of the ground.

$$H_{M,t} = I_{M,t} \cdot \frac{1+\cos\beta}{2} + \rho \cdot I_{H,t} \cdot \frac{1-\cos\beta}{2} \quad (4)$$

$$\cot\beta = \cos\varphi \cdot \cot\omega + \sin\varphi \cdot \mathrm{cosec}\omega \cdot \tan\delta \quad (5)$$

3.1.2 Power balance

Equation (6) is a power balance equation. $P_{fc,t}$, $P_{pv,t}$ and $P_{bt,t}$ on the left-hand-side in the equation are the PEFC power, photovoltaic power, and battery power, respectively. $P_{need,t}$, $P_{btc,t}$, $P_{loss,t}$ on the right-hand side in the equation represent power demand, the amount of battery charge, and loss of power, respectively. Charge-and-discharge loss of a battery is included in the power loss $P_{loss,t}$.

$$P_{fc,t} + P_{pv,t} + P_{bt,t} = P_{need,t} + P_{btc,t} + P_{loss,t} \quad (6)$$

3.2 Heat balance

Equation (7) is a heat balance equation.

$H_{fc,t}$, $H_{bl,t}$ and $H_{st,t}$ on the left-hand-side in the equation are the heat power of a fuel cell, a boiler, and a heat storage tank, respectively. $H_{need,t}$, $H_{sts,t}$ and $H_{loss,t}$ on the right-hand side of the equation are heat demand, the amount of heat storage, and the heat loss, respectively. Heat storage loss is included in the heat loss $H_{loss,t}$ on the right-hand-side of the equation.

$$H_{fc,t} + H_{bl,t} + H_{st,t} = H_{need,t} + H_{sts,t} + H_{loss,t} \quad (7)$$

3.3 Optimal analysis using GA

3.3.1 Objective function

If $P_{fc,t}$ in Eq. (6) and $H_{bl,t}$ in Eq. (7) are determined, the heating value of LPG $Q_{fuel,t}$ consumed by a compound microgrid is calculable. Here, the amount of fuel with the output power of $P_{fc,t}$ and $H_{bl,t}$ is decided by the PEFC power generation efficiency and the thermal efficiency of the boiler. Equation (8) defines the objective function in this study. The objective function minimizes the system fuel consumption $Q_{system,day}$ on one day. The fuel consumption $Q_{fuel,t}$ of the system from sample time t to $t+1$ is the sum of the fuel consumption $Q_{fc,t}$ of a fuel cell, and the fuel consumption $Q_{bl,t}$ of a boiler.

$$Q_{system,day} = \sum_{t=0}^{23} Q_{fuel,t} = \sum_{t=0}^{23} \left(Q_{fc,t} + Q_{bl,t} \right) \quad (8)$$

3.3.2 Optimal operation planning algorithm

In this study, the optimal operation plan of the proposal compound microgrid is analyzed using a GA. Figure 4 shows the operation optimization algorithm developed in this paper, and the analysis flow is explained below.

(1) The energy demand pattern data, equipment specifications, GA parameters, numerical weather data, efficiencies, initial conditions and system loss are used as input into a computer (system controller) in Calculation (A) in Fig. 4.

(2) In Calculation (B), many initial generation chromosome models are generated at random. One individual of the chromosome model expresses PEFC operation and power. The PEFC operation is represented with a 1 bit binary number and the PEFC power is represented by a 14 bit binary number.

(3) In Calculation (F), the PEFC power is determined by decoding the chromosome model. Furthermore, in Calculation (G), the production of electricity of photovoltaics is calculated using NWI (Section 3.1.1).

(4) In Calculations (H) through (K), battery, heat storage tank, and boiler operations are planned based on the power balance and heat balance equations (Section 3.1.2 and Section 3.2).

(5) The fuel consumption is calculable from the amount of PEFC and boiler power. In Calculation (L), these values are totaled, and the fuel consumption of the system in the sampling time t is determined.

(6) Calculations (E) through (M) are repeated from sampling time 0 to 23 for one chromosome model. In Calculation (N), the adaptive value (namely, the objective function shown in Eq. (8)) of the chromosome model is obtained from this result.

(7) The adaptive value of all the chromosome models is decided by repeating Calculations (D) through (O). The ranking of the chromosome models is decided according to the magnitude of the adaptive value of each chromosome (Calculation (P)).

(8) The chromosome models with low adaptive value are selected, and they are exchanged for the new randomly generated model. Moreover, the genetic manipulation of crossover and mutation is added based on the probability given in Calculation (A) concerning the chromosome models with high adaptive value (Calculation (Q)).

(9) Calculations (D) through (Q) (repeated calculation of Calculations (C) to (R)) are repeated for a defined number of generations. In the last generation's chromosome group, the solution with the highest adaptive value is chosen to be the optimal system operation plan (Calculation (S)).

4. Case Analysis

4.1 Equipment specifications

The equipment specifications for the case analysis of the PEFC and photovoltaics compound microgrid are shown in Table 1. The microgrid assumes that the equipment is installed in Sapporo, Japan (latitude 43.062-degree north and longitude 141.354-degree east, a cold and snowy area).

(1) PEFC with a reformer

The maximum PEFC power with a reformer is 3 kW, and this performance is shown Fig. 3.

(2) Photovoltaics

The maximum efficiency and photovoltaic temperature coefficients are 16.4% and 0.4%/K, respectively. These values are general facility values used in Japan. The solar panel is installed in the roof, with a slope of 30-degrees facing south. Moreover, the solar cell area is set to 60.0 m^2.

The area of the general solar cell installed into individual houses in Japan is usually 25 m^2 to 40 m^2 (for a solar cell with a 3 kW to 5 kW capacity).

(3) Battery, converter and inverter

The self-discharge of a battery is set to 10% per hour. The converter and inverter efficiencies are both set to 95%.

(4) Heat storage tank and boiler

Heat dissipation loss of a heat storage tank is set to 5% per hour, and the boiler efficiency is set to 90%.

4.2 GA parameters

The GA parameters in the proposed algorithm are shown in Table 2. These values were chosen by repeating trial and error so that the convergence solution was as stable as possible. Since the convergence solution (analysis result) has dispersion for every analysis, the optimal solution is obtained by repeating the same analysis.

4.3 Energy demand pattern

Power and heat are supplied to three individual houses in Sapporo, Japan using the proposed microgrid. Figure 5 shows the power and heat demand on a representative day every month [11]. There is no cooling load and heating is included in the heat load. Therefore, the power load pattern on a representative day of every month does not vary significantly throughout the year. On the other hand, the magnitude of demanded heat varies greatly between the summer season and winter season.

4.4 Error of the NWI

Various error characteristics of the NWI can be considered. However, the investigated case various NWI errors were not found. Accordingly, the error pattern of the following two types is installed in this study. Figure 6 shows the error pattern of the two types used to analyze the proposed algorithm (Fig. 4). As shown

in Fig. 6 (a), a linear- -error and a quadratic error are installed as error patterns. Target day operation plans are determined by the NWI at 0:00 on the target day. In this paper, the error that is proportional ($error_t = const1 \cdot t$) to time is defined as the linear error. On the other hand, the error that follows ($error_t = const2 \cdot t^2$)a secondary curve relative to time is defined as the quadratic error. Here, the integrated values of the two error types are set equal to each other. Therefore, $const1$ and $const2$ were decided so that Area A and Area B (shown in Fig. 6 (a)) might become equal (in Fig. 6 (a), Area A=Area B=1.0). The common characteristic of these error patterns is the increase of the NWI error as time increases. Moreover, as shown in Figs. 6 (b) and (c), fluctuation errors of ±20% and ±40% at random are added to the two error types. These fluctuation errors simulate the instability of the solar insolation data.

5. Results and Discussion

5.1 Operation planning

Figure 7 shows the results of the system operation plan optimization analysis on representative February days (winter). Figures 7 (a) and (b) are the optimal operation plans for a power system and a heat system, respectively. Moreover, Fig. 7 (c) shows the fuel consumption plan in this case. The fuel consumption is the sum total of each value of a PEFC with a reformer and a boiler. Figure 8 shows the operation results of the system at the time of the linear error and quadratic error on the NWI. Similarly, Fig. 9 shows the results of the system operating plan optimization analysis on representative August days (summer season). Figure 10 shows the operation result with the two error types on the NWI.

The battery operation plans shown in Fig. 7 (a) and Fig. 9 (a) differ greatly for each month. Accordingly, the amount of the maximum electricity storage in August is clearly large compared with that in February. This is because of the difference in the photovoltaic power generation in February and August. Moreover, when Fig. 7 (b) is compared with Fig. 9 (b), the ratios of the PEFC exhaust heat to heat demand vary greatly for each month. The PEFC exhaust heat to the heat demand ratio is very low in February. As a result, heat supply on February representative days is mainly boiler heat. The summer season has little system fuel consumption based on the difference in the heat power of a boiler (Fig. 7 (c) and 9 (c)). Therefore, if the

proposed compound microgrid is optimized based on the objective function in Eq. (8), power should be generally optimized in the summer and heat should be generally optimized in the winter.

5.2 Influence of the numerical weather information error

The relation between the NWI error and the power system operation results is investigated (Fig. 8 and Fig. 10). If an error is included in the NWI, the amount of storage of electricity will increase sharply for any month. From this result, the time shift of power is conjectured to perform an important role for optimizing system operation with NWI error. Accordingly, because the operation plan is strongly influenced by battery capacity setup , it is thought that the fuel consumption of the system changes greatly.

When installing the linear error into the NWI, large battery capacity is required compared with the quadratic error. Therefore, the system operation method changes with the error characteristics of the NWI. To minimize the battery capacity, the NWI quadratic error is desirable.

5.3 Fuel consumption

Figure 11 (a) shows the fuel consumption plan in the case of the optimal system operation plan. Moreover, Figs. 11 (b) and (c) show the operation results of the fuel consumption with NWI error. The winter season (February and December) with the large heat power of a boiler requires significant fuel consumption. Moreover, when Figs. 11 (b) and (c) are compared with the fuel consumption pattern for every month, shown in Fig. 11 (a), there is a clear difference. Accordingly, the total fuel consumption on the representative day was calculated about every month (Fig. 12). As shown in Fig. 12, the results of the fuel consumption plan in the optimal system operation plan and the fuel consumption when operating the system with NWI error were small in value. From this result, it is surmised that installing operation optimization using the NWI in the fuel cell microgrid with unstable photovoltaics achieves good operation. Even if it includes error in the NWI, the system maintains good operation and hardly suffers from the error.

6. Conclusions

In this paper, the photovoltaic electricity production was predicted using numerical weather information (NWI), and a system operation optimization algorithm based on NWI was proposed. The proposed algorithm

uses a GA (genetic algorithm), and optimizes the system operation plan . However, since error exists between NWI and meteorological data in real time, the operation of an actual system differs from the optimal operation plan defined beforehand. Accordingly, in this paper, the relation between the error characteristic of the NWI and fuel consumption of the system were clarified. Moreover, the following was concluded. First, when the proposal compound microgrid is installed in a cold region and optimized, power is mainly optimized in the summer and heat is primarily optimized in the winter. Second, for system operation with NWI error, the power time shift has an important role. Accordingly, the operation plan changes greatly with the magnitude of the battery capacity. As a result system fuel consumption varies greatly from month to month. Lastly, high-performance operation can be achieved by installing the operation optimization method based on the NWI into the fuel cell microgrid with unstable photovoltaics. Even if the error shown in this paper is included in the NWI, the influence on the system fuel consumption is small.

Nomenclature

H	:	Heat	W
I_D	:	Direct solar radiation intensity	W/m^2
I_H	:	Global-solar-radiation intensity	W/m^2
I_M	:	Horizontal sky solar radiation intensity	W/m^2
H_D	:	Intensity of direct solar	W/m^2
H_M	:	Intensity of sky solar radiation	W/m^2
P	:	Power	W
Q	:	Fuel consumption	W
R_T	:	Temperature coefficient	%/K
S_s	:	Area of the solar cell	m^2
T	:	Temperature	K
T_c	:	Temperature of the solar cell	K
T_o	:	Reference temperature	K
t	:	Sample time	

Greek Symbols

β : Angle of the acceptance surface gradient

δ : The solar celestial declination

φ : The latitude of a setting point

η_s : Photovoltaics efficiency at T_o %

θ : Incident angle to the sunlight acceptance surface

ρ : Ground reflection factor

ω : Hour angle

Subscripts

bl : Boiler

bt : Battery

btc : Battery discharge

fc : PEFC with reformer

loss : Energy loss

need : Energy demand

pv : Photovoltaics

s : Solar module

st : Heat storage

sts : Heat storage output

Acknowledgements

This work was partially supported by a Grant-in-Aid for Scientific Research (C) from JSPS.KAKENHI (20560204).

References

[1] Shin'ya Obara, Equipment plan of compound interconnection micro-grid composed from diesel power plants and solid polymer membrane-type fuel cell, International Journal of Hydrogen Energy, Vol. 33, No. 1, (2008) 179-188.

[2] Hirohisa Aki, Shigeo Yamamoto, Junji Kondoh, Tetsuhiko Maeda, Hiroshi Yamaguchi, Akinobu Murata, Itaru Ishii, Fuel cells and energy networks of electricity, heat, and hydrogen in residential areas, International Journal of Hydrogen Energy, Vol. 31, No. 8, (2006) 967-980.

[3] Huang Jiayi, Jiang Chuanwen, Xu Rong, A review on distributed energy resources and MicroGrid, Renewable and Sustainable Energy Reviews, Vol. 12, No. 9, (2008), 2472-2483.

[4] S. Obara, Load response characteristics of a fuel cell micro-grid with control of number of units, International Journal of Hydrogen Energy, Vol. 31, No. 13, (2006), 1819-1830.

[5] Shin'ya OBARA, Operating Schedule of a Combined Energy Network System with Fuel Cell, International Journal of Energy Research, Vol. 30, No. 13, (2006) 1055-1073.

[6] Shin'ya OBARA, Equipment Arrangement Planning of a Fuel Cell Energy Network Optimized for Cost Minimization, Renewable Energy, Vol. 32, No. 3, (2007) 382-406.

[7] Shin'ya OBARA, The Exhaust Heat Use Plan when Connecting Solar Modules to a Fuel Cell Energy Network, Transactions of the ASME, Journal of Energy Resources Technology, Vol. 129, No. 1, (2007) 18-28.

[8] Online data service, GPV/GSM (Grid Point Value / GSM (Global Spectral Model)), http://www.jmbsc.or.jp/hp/online/f-online0a.html, Japan meteorological business support center, 2009.

[9] Data of Japan Meteorological Agency, http://database.rish.kyoto-u.ac.jp/arch/jmadata/gpv-original.html, Kyoto University, 2009.

[10] Development of home fuel cell cogeneration system in Tokyo Gas, ALIA News Vol. 89, http://www.alianet.org/homedock/15kinen/5-2.html, 2009.

[11] K. Narita, "Research on unused energy of cold region cities and utilization for district heat and cooling," Ph.D. thesis, Dep. Socio-Environmental Eng. Faculty of Eng., Hokkaido Univ. Sapporo, Japan, 1996.

Captions

Fig. 1. System scheme

Fig. 2 System operation plan of the compound microgrid with a PEFC and photovoltaics with predicted electricity production

(a) Predicted solar power and power demand

(b) PEFC power generation

(c) Battery operation

(d) Heat demand

(e) PEFC exhaust heat

(f) Heat storage and boiler operation

Fig. 3 Efficiency characteristics of the PEFC with steam reformer

(a) Power generation efficiency

(b) Heat generation efficiency

Fig. 4 Optimal operation algorithm

Fig. 5 Energy demand model. Load patterns for three individual houses on representative days in Sapporo, Japan.

(a) Power demand model

(b) Heat demand model

Fig. 6 Error function and error function with random error in the numerical weather information

(a) Error function

(b) Error of the numerical weather information ±20%

(c) Error of the numerical weather information ±40%

Fig. 7 Analysis results of the proposed microgrid operation plan in February

(a) Operation planning of the power system

(b) Operation planning of the heat system

(c) Fuel consumption

Fig. 8 Operation planning in the case of numerical weather information with two types of error; a power system in February.

(a) Linear error

(b) Quadratic error

Fig. 9 Analysis results of the operation planning of the proposed microgrid in August

(a) Operation planning of the power system

(b) Operation planning of the heat system

(c) Fuel consumption

Fig. 10 Operation planning in the case of numerical weather information with two error types; power system in August.

(a) Linear error

(b) Quadratic error

Fig. 11 Analysis results of the fuel consumption

(a) Optimal operation planning

(b) In the case of a numerical weather information with ±20% error

(c) In the case of a numerical weather information with ±40% error

Fig. 12 Analysis results of the fuel consumption on a representative day

Table 1 Equipment specifications

Table 2 GA parameters

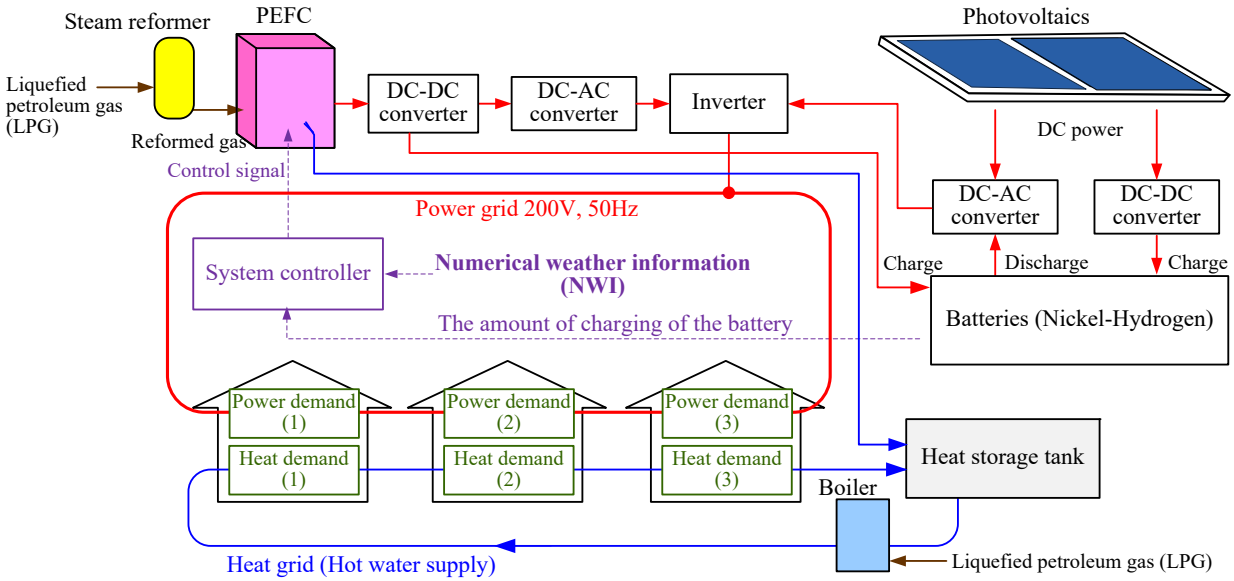

Fig. 1. System scheme

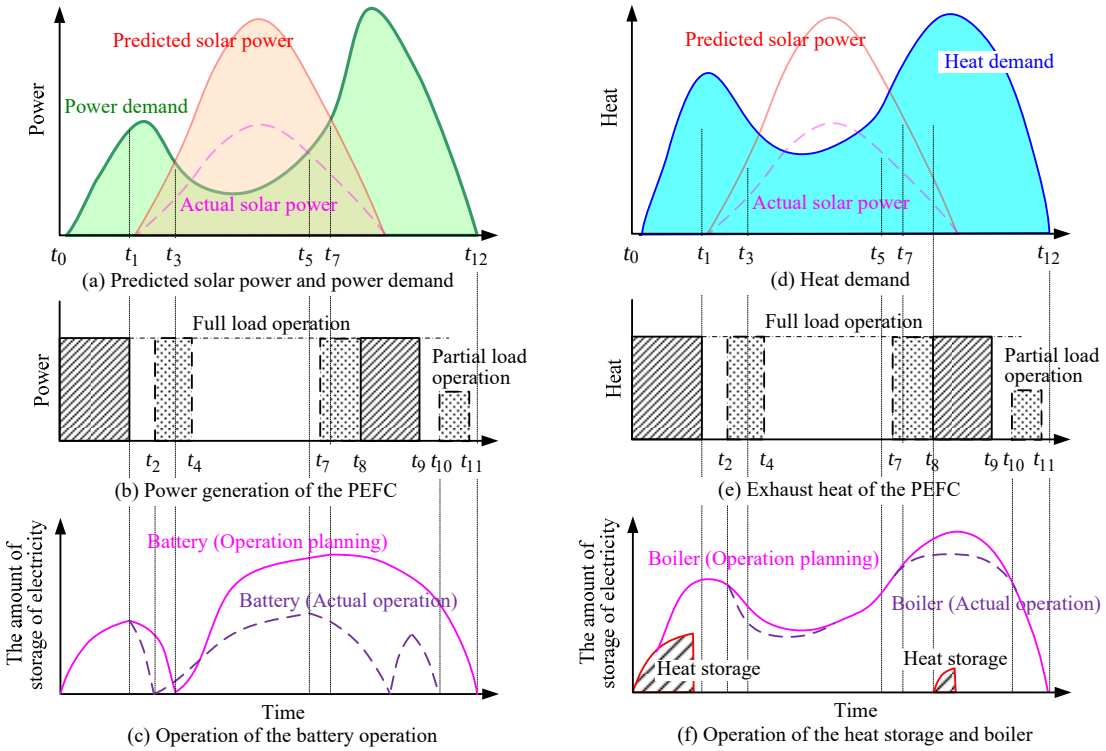

Fig. 2 System operation planning of The compound microgrid installation of a PEFC and photovoltaics with prediction of the production of electricity

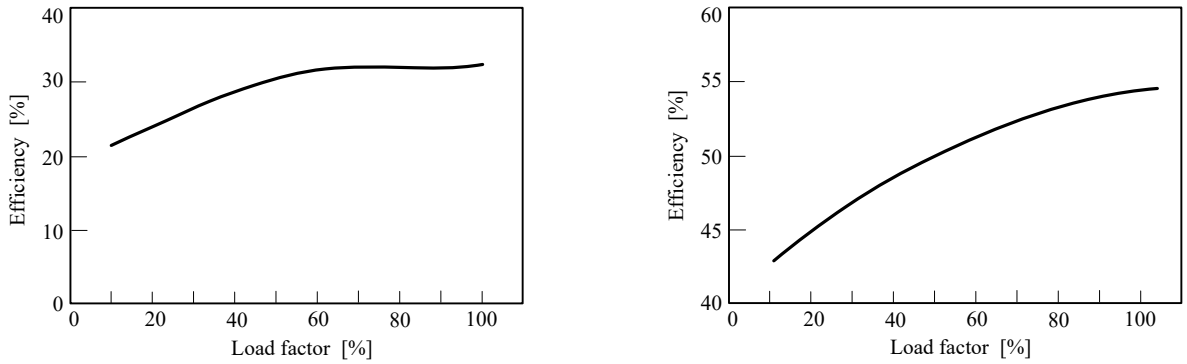

(a) Power generation efficiency (b) Heat generation efficiency

Fig. 3 Efficiency characteristics of the PEFC with steam reformer

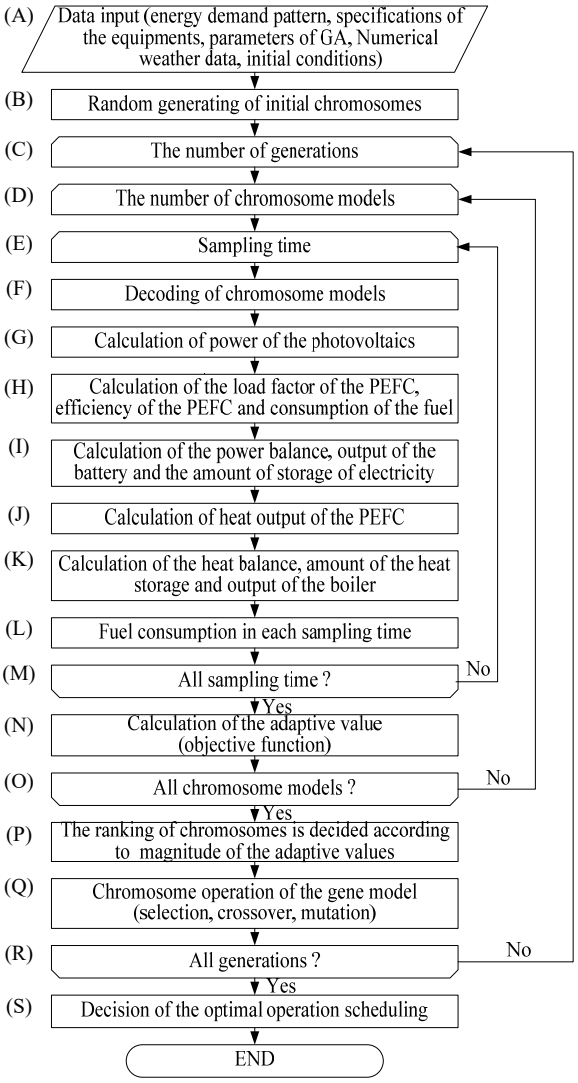

Fig. 4 Optimal operation algorithm

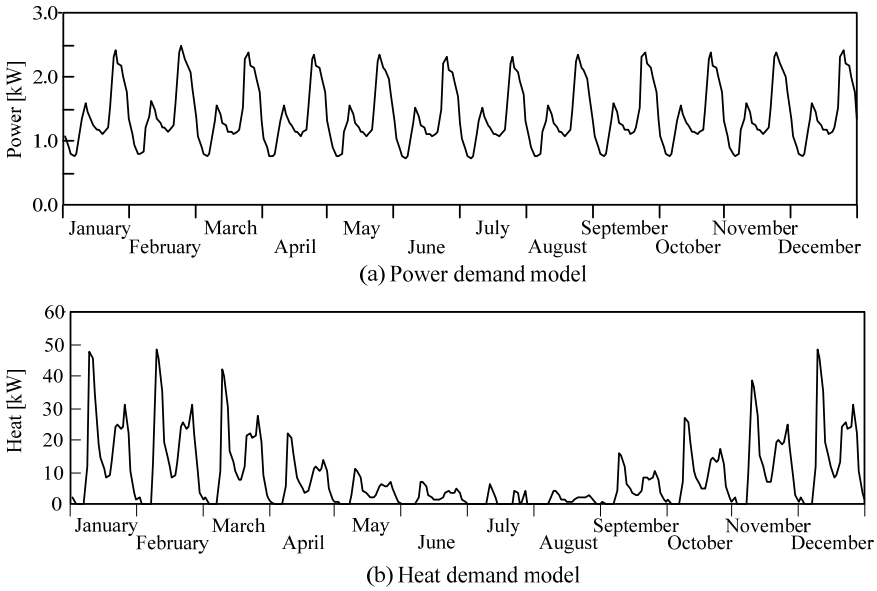

(a) Power demand model

(b) Heat demand model

Fig. 5 Energy demand model. Load patterns concerning three individual houses of the every month representative days in Sapporo.

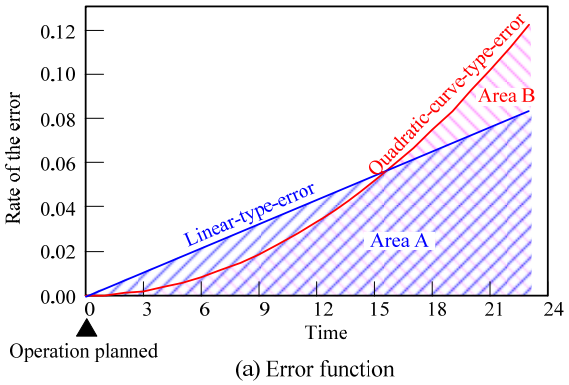

(a) Error function

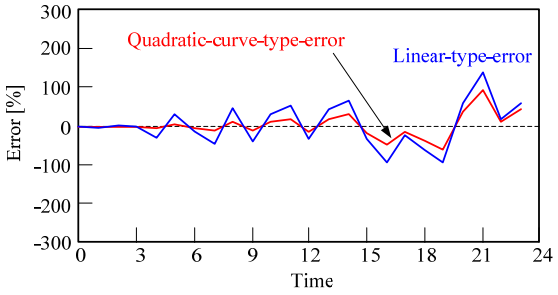

(b) Error of the numerical weather information ±20 %

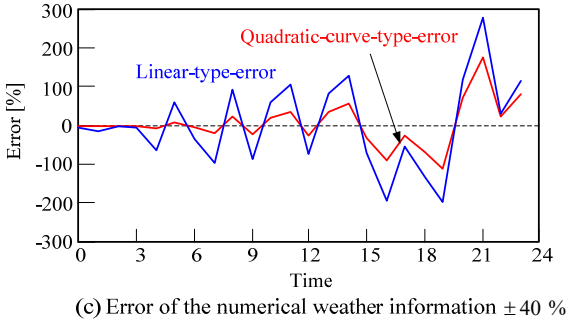

(c) Error of the numerical weather information ±40 %

Fig. 6 Error function and error function with random error of the numerical weather information

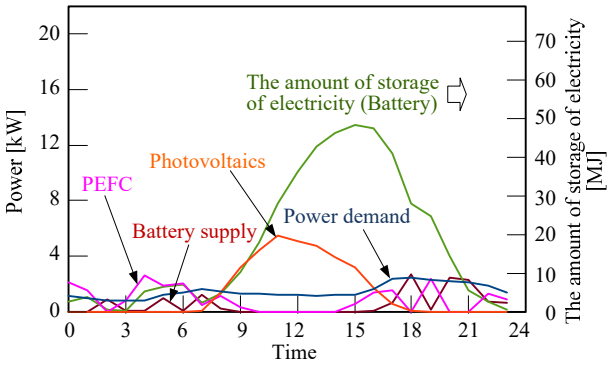

(a) Operation planning of the power system

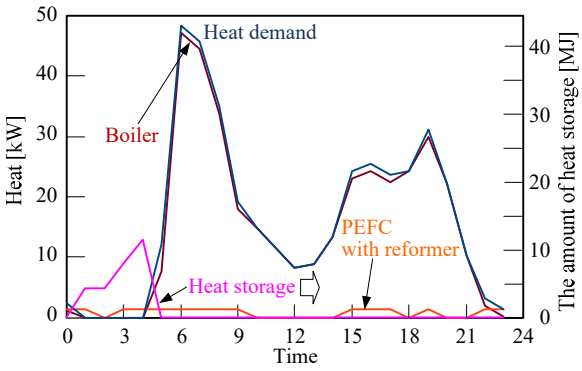

(b) Operation planning of the heat system

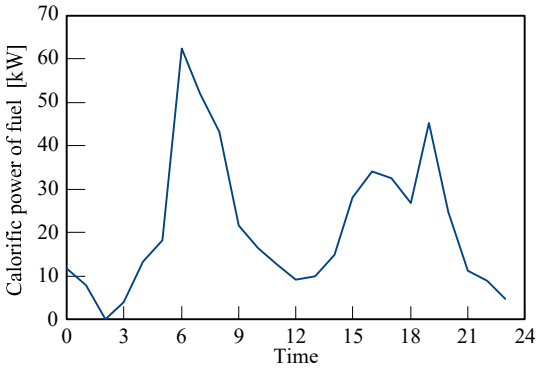

(c) Fuel consumption

Fig. 7 Analysis results of the operation planning of the proposal microgrid in February

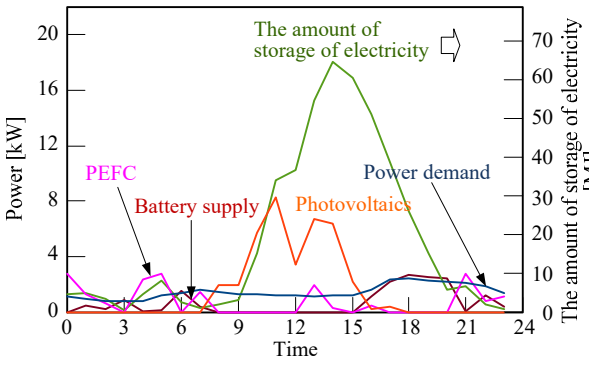

(a) Linear-type-error

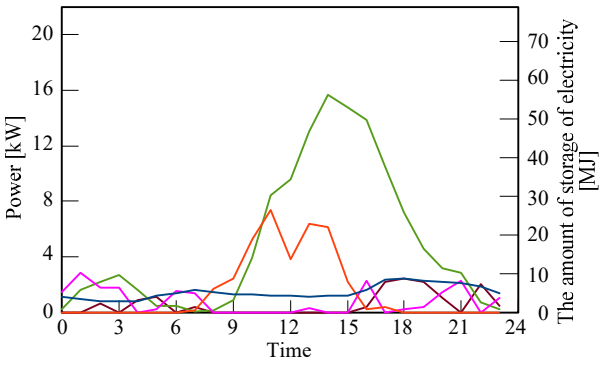

(b) Quadratic-curve-type-error

Fig. 8 Operation planning in the case of a numerical weather information with two types error ±40 %. Power system, in February.

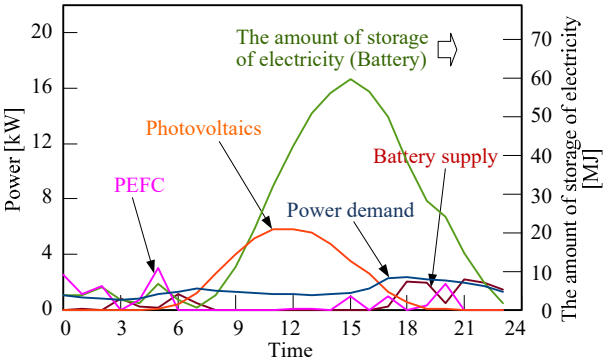

(a) Operation planning of the power system

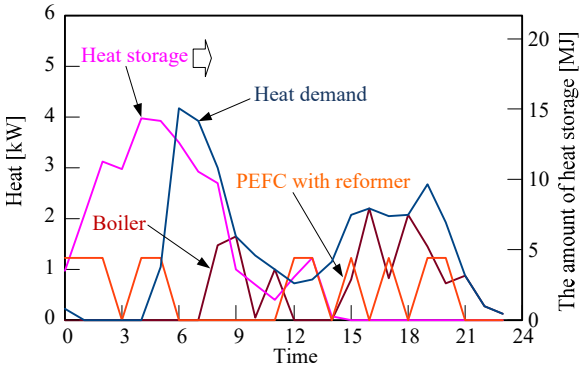

(b) Operation planning of the heat system

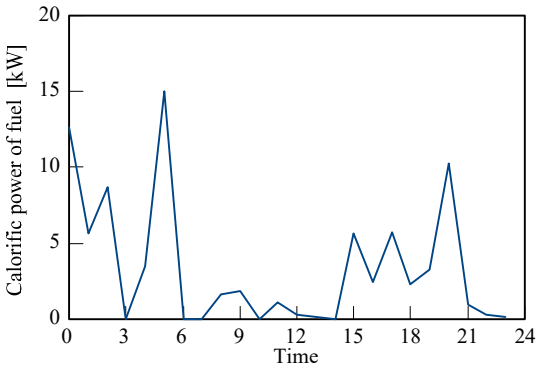

(c) Fuel consumption

Fig. 9 Analysis results of the operation planning of the proposal microgrid in August

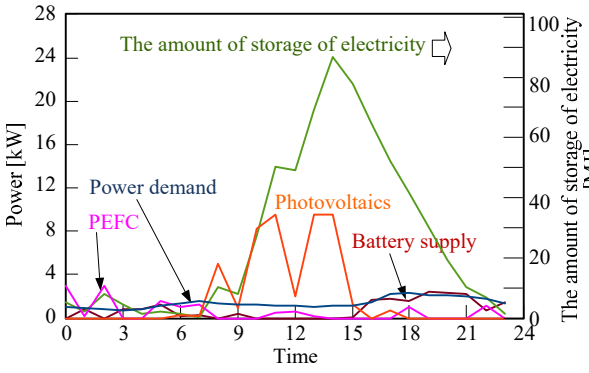

(a) Linear-type-error

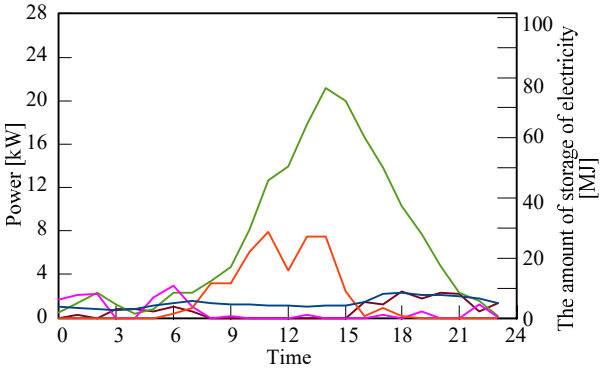

(b) Quadratic-curve-type-error

Fig. 10 Operation planning in the case of a numerical weather information with two types error ±40%. Power system, in August.

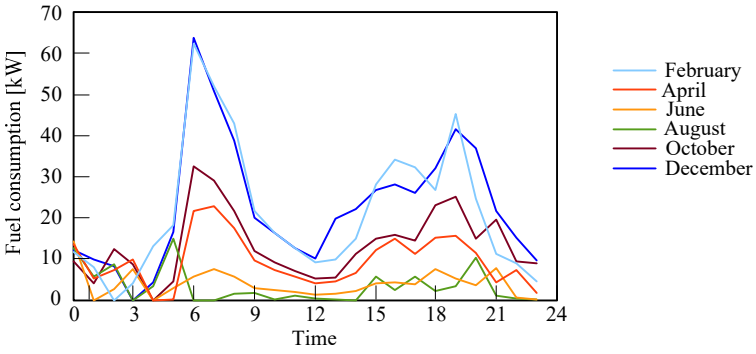

(a) Optimal operation planning

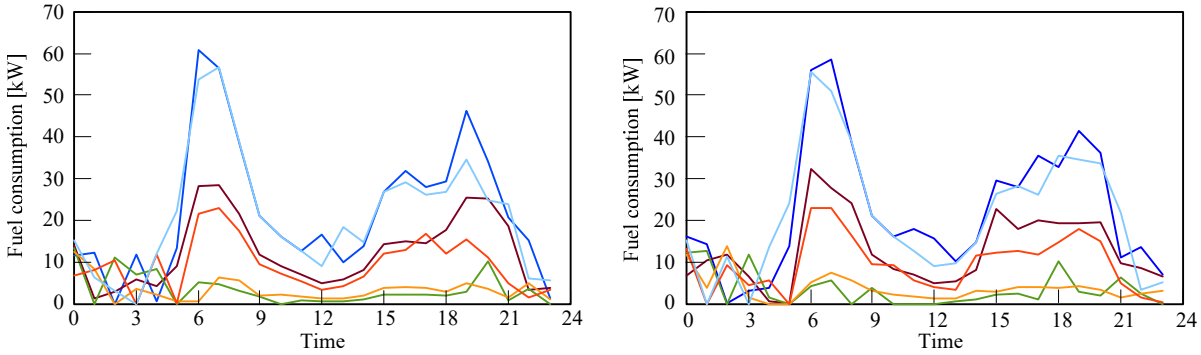

(b) In the case of a numerical weather information with ±20% error

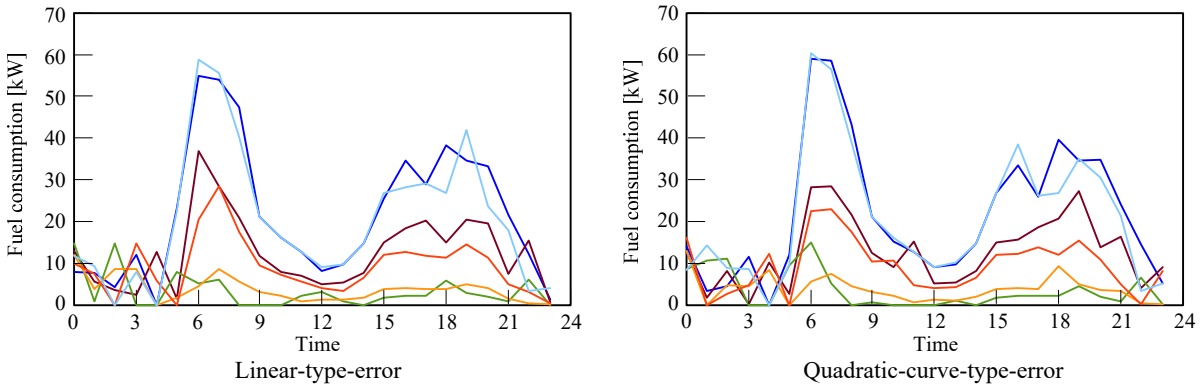

(c) In the case of a numerical weather information with ±40% error

Fig. 11 Analysis results of the fuel consumption

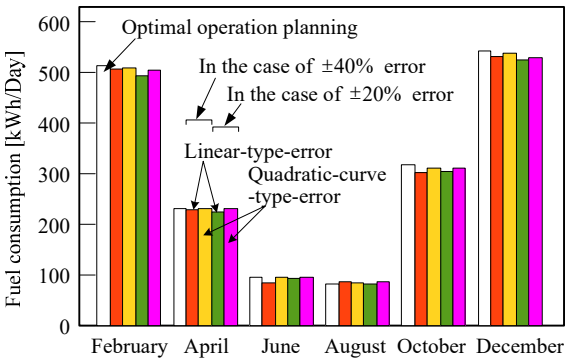

Fig. 12 Analysis results of the fuel consumption in representative day

Table 1 Specification of equipments

- PEFC maximum power	3 kW
- PEFC performance	Fig. 3
- Solar cell type	Multicrystalline silicon
-Area of solar cell	60.0 m^2
- Maximum generation efficiency of the solar cell	16.4 %
- Temperature coefficient of the solar cell	0.4 %/K
-Battery type	Nickel-Hydrogen
-Amount of battery self-discharge	10 %/hour
-Efficiency of converter	95 %
-Efficiency of inverter	95 %
-Loss of heat storage	5 %/hour
-Efficiency of boiler	90 %

Table 2 GA parameters

- Then umber of chromosome models	10000
- Generation number	100
- Probability of mutation	10 %
- Selection	50% of a low rank is replaced